FF

ISSN/1120-5563

ENTE PER LE NUOVE TECNOLOGIE
L'ENERGIA E L'AMBIENTE

Dipartimento Energia

AN IMPROVED MULTIPLE SCATTERING MODEL FOR CHARGED PARTICLE TRANSPORT

A. FERRARI, P. R. SALA, R. GUARALDI, F. PADOANI

RT/ERG/93/26

ISSN/1120-5563

ENTE PER LE NUOVE TECNOLOGIE
L'ENERGIA E L'AMBIENTE

Dipartimento Energia

AN IMPROVED MULTIPLE SCATTERING MODEL FOR CHARGED PARTICLE TRANSPORT

A. FERRARI, P. R. SALA,
INFN - Sezione di Milano

R. GUARALDI, F. PADOANI
Centro Ricerche ENEA "E. Clementel" di Bologna

RT/ERG/93/26

Testo pervenuto nel novembre 1993

An improved multiple scattering model for charged particle transport

A. Ferrari, P.R. Sala, R. Guaraldi and F. Padoani

An extended model for charged particle transport through the multiple scattering formalism based on the Molière theory has been developed (by A.F. and P.S.). The new model has been implemented independently through two different algorithms in the Monte Carlo codes FLUKA (used predominantly in high energy applications for transport of hadrons and leptons) and MCNPE-BO (based on MCNP3a and employed in the field of radiation protection and dosimetry). The codes are currently being benchmarked on a variety of reference problems in their respective fields of application.

1. Introduction

An extended model for charged particle transport through the multiple scattering formalism based on the Molière theory has been developed at INFN. The aim of this model is to provide a reliable and possibly user-friendly algorithm for Monte Carlo simulations of charged lepton and hadron transport. Care has been taken in accounting also for effects which are usually not included in standard multiple scattering algorithms but which can become significant at very high energies and/or at very grazing angles.

The new model has been implemented independently through two different algorithms in the Monte Carlo codes FLUKA [1] and MCNPE-BO, codes developed at INFN and ENEA, respectively. Both these codes were originally based on EGS4 [2] for electron and positron transport (FLUKA also for the photon transport).

In the following, after a description of the model, some benchmarks of the codes are presented. All the benchmarks refer to low–medium-energy electron problems which both codes are able to cope with (and usually these are the most sensitive ones to the multiple scattering effect); however, one of the codes (FLUKA) is primarily designed for modelling the interactions of high energy beams with matter and therefore the model has been developed bearing in mind also these applications.

2. The reasons for a new model

There are two possible approaches to the modelling of charged particle multiple scattering in a condensed history Monte Carlo. The first one is based on the theory developed by Molière [3,4] and slightly modified by Bethe [5], the second one is based on the theory developed by Goudsmit and Saunderson [6]. The Molière theory makes use of the small angle approximation to derive a multiple scattering distribution which is valid provided the number of elementary scatterings is large enough (> 20). The underlying single scattering cross section is the Rutherford one corrected for screening according to an expression derived by Molière himself. The Goudsmit and Saunderson theory does not contain such limitations and supplies the multiple scattering distribution as an expansion where any single scattering cross section can be inserted. Despite the underlying approximations the Molière theory has many advantages when used for simulating charged particle transport in arbitrary geometries with arbitrary step lengths since it can be expressed with universal functions using just a few material and particle dependent parameters. Furthermore this theory is in principle able to describe the distribution function of any single physical quantity of interest [4] (polar scattering angle, projected angle, position angles, lateral displacement

etc.), even though it does not provide any means for computing the joint distribution of two or more of these quantities. Both theories are expressed as a function of the total path length travelled by the particle. Therefore, as soon as the particle step length is not extremely short, suitable "wiggliness" corrections must be introduced to take into account the difference between the straight and the curved path length and possibly also between the actual displacement direction and the original direction of motion of the particle. Both corrections can be quite important unless severe limitations on step lengths are adopted.

The default electron/positron transport algorithm of EGS4 makes use of the Fermi–Eyges–Yang theory [7] to compute an average straggling correction to the travelled step length, and no correction is made to the original particle direction when performing the step. This algorithm behaves poorly, mainly because the wiggliness correction is grossly overestimated as demonstrated in ref. [8]. As a consequence results are strongly step length dependent and meaningful results can be obtained only by adopting very small step lengths. A partial solution to this problem is implemented into EGS4 [9] and consists of a set of constraints on the maximum step length, the main one being a restriction on the maximum fraction of energy lost per step. However, this limitation implies a severe CPU penalty and does not always solve the problem. In particular for heavy materials it may occur that the convergence to the correct answer cannot be reached before steps become so short that they turn off the multiscattering algorithm. A detailed discussion of these problems can be found in refs. [8,9], concerning mainly low–medium-energy beams. Examples of the sensitivity to step length of results computed with high energy beams can be found in refs. [10,11]; it should be pointed out that these examples clearly show the difficulty of using the code as a predictive tool if no known experimental answer is available to tune the step length parameters to the given problem. The need for satisfactory simulations of electron/positron transport within reasonable CPU times calls for a different transport algorithm. An algorithm names PRESTA [8,12] has been proposed as a possible solution to the above mentioned problems. Results presented in the literature [8,12] for this algorithm are quite promising. However, in our judgment there may be some limitations to this model:

a) The Molière theory is used well beyond its range of validity, including situations in which the distribution function takes negative values.

b) No account is made for the variation with energy of the screening correction, which is fixed to its asymptotic value for $v = c$. This approximation overestimates both the scattering of the lowest energy electrons and the range of validity of the theory, leading to incorrect results at low energies and/or for heavy materials. It cannot be used for hadrons and muons.

c) Whilst the lateral displacement applied to the trajectory fully correlates with the final deflection angle, the longitudinal one does not, leading to the physically unacceptable result that, for a given total path length, particles undergoing the largest deflections also make the longest straight steps.

d) No account is made for corrections to the Molière single scattering cross section (e.g. spin-relativistic and nuclear form factors).

It is likely that these limitations should show up only in specific problems, such as backscattering problems: indeed in ref. [12] there are indications that the algorithm does not work properly in this field.

3. The adopted model

Deriving a solution still based on the Molière theory but without the limitations of the original EGS4 algorithm, and that can also be applied to charged hadrons and muons, gave rise to the model that will be described in the following. The specific goals underlying its derivation are:

- to achieve an acceptable step length insensitivity, both to allow long steps to save CPU time and to avoid the predictivity properties of the model to be degraded;
- to account for correlations as far as possible;
- to possibly account for the spin-relativistic corrections to the Rutherford cross section which are not included in the Molière derivation;
- to account for the effect of nuclear form factors, which is particularly important for hadrons and muons;
- not to spoil the intrinsic advantage of the Molière theory, that is that any correction has to be implemented through simple particle and material independent functions.

The model is composed principally of two parts, the path length correction algorithm (from this point referred to as the PLC) and the correlation algorithm for the various angles involved in each step simulation. It has been implemented at different levels in the two codes, in its full derivation in FLUKA, without the correlations in MCNPE-BO, but with an improved treatment of the PLC which should allow a very high level of step-length insensitivity. A description of the model and a few examples of its performance are described in the following. Particular emphasis will be given to backscattering problems to demonstrate the validity of the Molière theory when properly used also in this field.

3.1. A brief summary of the Molière theory

A description of the quantities used in the following is given below. The z-axis is the axis of the original motion of the particle and the following quantities describe the particle position and direction at the end of a step:

θ is the polar angle of the velocity vector (with respect to the z-axis);
η is the polar angle of the particle position vector;
Φ is the projected angle of the velocity vector on a plane containing the z-axis;
Ψ is the projected angle of the position vector on a plane containing the z-axis;
ϕ is the azimuthal angle of the velocity vector;
ω is the azimuthal angle of the position vector;
$\Delta\omega = \omega - \phi$ is the azimuthal angle between the velocity and the position vectors;
κ is the angle between the position and velocity vectors;
t is the total curved path travelled by the particle;
p is the modulus of the position vector;
x, y, s are the coordinates of the final position.
The following relation hold:

$$\begin{aligned}
&\tan\Phi = \tan\theta\cos\phi,\\
&\tan\Psi = \tan\eta\cos\omega,\\
&\cos\kappa = \cos\eta\cos\theta + \sin\eta\sin\theta\cos\Delta\omega,\\
&s = p\cos\eta,\\
&x = p\sin\eta\cos\omega,\\
&y = p\sin\eta\sin\omega.
\end{aligned} \tag{1}$$

Usually the PLC is defined with respect to the particle displacement along the original direction of motion (s in the present notation), that is

$$\mathrm{PLC} = \frac{t - \langle s\rangle}{t}.$$

However, the particle is displaced at each step by a quantity p along a direction which is not necessarily the original one. Therefore a wiggliness correction of more direct physical interpretation can also be computed with respect to p: this correction is smaller than the PLC ($s \le p \le t$ of course) and it is used in the proposed algorithm as explained in section 3.5.

The Molière theory can be characterized by the quantities

$$\begin{aligned}
&\Omega_0 = b_c t/\beta^2,\\
&B - \ln B = b = \ln\omega_0,\\
&\chi_r = \chi_c B^{1/2},\\
&\chi_c = \frac{\chi_{cc} t^{1/2}}{E\beta^2}.
\end{aligned} \tag{2}$$

χ_{cc}, b_c are the only material dependent quantities, given by

$$\chi_{cc} = \left[\frac{4\pi n z^2 Z(Z+\xi_e)e^4}{c^4}\right]^{1/2},$$

$$b_c = \frac{0.855^2\chi_{cc}^2\hbar^2}{1.167^2 m_e c^2 e^4 Z^{2/3}(1.13 + (3.76\alpha^2 z^2 Z^2)/\beta^2)},$$

where n is the number of atoms per unit volume, z and Z are the atomic numbers of projectile and target, ξ_e is a parameter taking into account the scattering on atomic electrons, and α is the fine structure constant. The distribution for θ is given in terms of the scaled variable θ_r by

$$\begin{aligned}
&P(\theta, B)\,\mathrm{d}\theta = 2\pi\theta f_{\mathrm{mol}}(\theta_r, B)(\sin\theta/\theta)^{1/2}\,\mathrm{d}\theta_r,\\
&\theta_r = \theta/\chi_r,\\
&\chi_r = \chi_c B^{1/2},\\
&f_{\mathrm{mol}}(x, B) = \frac{1}{2\pi}\left(f_0(x) + \frac{f_1(x)}{B} + \frac{f_2(x)}{B^2}\right),
\end{aligned} \tag{3}$$

whilst the distribution for η is given by [4]

$$\begin{aligned}
&P(\eta, B^*)\,\mathrm{d}\eta = 2\pi\eta f_{\mathrm{mol}}(\eta_r, B^*)\left(\frac{\sin\eta}{\eta}\right)^{1/2}\mathrm{d}\eta_r,\\
&B^* - \ln B^* = b - \Delta b = b + 2/3 - \ln 3,\\
&\eta_r = \eta/\chi_r^*,\\
&\chi_r^* = \chi_c\sqrt{B^*/3}.
\end{aligned}$$

Note that the term $(\sin\theta/\theta)^{1/2}$, which represents the Bethe correction derived for θ, is here applied in an analogous fashion also to η. The functions f_i in eq. (3) are expressed by definite integrals of analytical functions: the resulting f_0 is simply a Gaussian.

3.2. Range of applicability of the theory

The Molière theory can be reliably applied for step lengths involving a large number of elementary deflections but with an average deflection less than one radian. These conditions correspond roughly to $B > 4$ and $\chi_r < 1$. For heavy elements there exists a limiting energy below which the fulfillment of both conditions is impossible and the theory cannot be applied. The effective minimum energy depends somewhat on the exact expression for the screening correction applied to the single scattering cross section. The validity of the energy dependent term derived by Molière, $(3.76/1.13)(\alpha^2 z^2 Z^2/\beta^2)$, is in fact questionable (see the discussion in ref. [13] and the empirical correction applied in ETRAN [14], which is also adopted in FLUKA).

3.3. The average path length correction and its variance

The evaluation of the average path length correction is accomplished in a very standard way by evaluat-

ing the average displacement $\langle s \rangle$ along the original direction, starting from the equation

$$\langle s \rangle = \int_0^t dt' \, \langle \cos \theta(t') \rangle \tag{4}$$

In evaluating eq. (4) only the Gaussian term f_0 is used, neglecting both f_1 and f_2; of course this will result in some inaccuracy for step lengths close to the minimum one allowed by the theory, even though the path length correction for these steps is usually very small. The computation of the contribution of the f_1 term to the average path length correction in a consistent manner is strongly influenced by the bounds on the scattering angle and by high order corrections to the Molière single scattering law. In fact, due to the original small angle approximation, the contribution of the f_1/B term (representing the single scattering tail of the distribution) to $\langle \theta^2 \rangle$ is strictly divergent. This contribution has been evaluated in ref. [8] taking into account only the bound $\theta \leq \pi$ and shown to be usually negligible. However, it should be pointed out that the inclusion of the f_1 contribution in the evaluation of the PLC is questionable when only an average wiggliness correction is used without any correlation with the deflection angle. Since the contribution f_1 originates mainly from relatively infrequent large angle scattering, when only an average correction is applied (as in ref. [8]), its inclusion would lead to an overestimation of the path length correction for most of the steps and to an underestimation for those occurring in such rare large deflections. It will be clear from the discussion of the following sections how the proposed algorithm tackles this problem through the inclusion of proper correlations between the wiggliness correction and the scattering angle. Forgetting this problem for the moment and retaining only the terms coming from f_0, after expanding all functions of θ up to order θ^4, the integral can be solved analytically, provided the Molière expression for B is extended for continuity down to $b, B = 1$ and a reasonable extrapolation for $\Omega_0 \to 0$ is adopted. No significant inaccuracy can be caused by these approximations since the contribution coming from the extrapolated interval is quite small and any smooth function adopted for $\langle \cos \theta(t) \rangle$ joining with continuity the Molière expression at $B \approx 4$ and going to 1 for $t \to 0$ would produce virtually the same numbers for $\langle s \rangle$. The result is given by

$$\langle s \rangle = t(1 - \mathrm{PLC}) = t\left[1 - \frac{\tau_1(B)}{2} X + \frac{\tau_2(B)}{6} X^2\right], \tag{5}$$

$$X = \chi_c^2 B = \chi_r^2,$$

where τ_1 and τ_2 are given by

$$\tau_1(B) = 1 - \frac{\sum_{k=1}^{\infty} \frac{(2B)^k}{kk!} + \ln B - 2.2173}{\Omega_0^2 B},$$

$$\tau_2(B) = 1 - \frac{2\sum_{k=1}^{\infty} \frac{(3B)^k}{kk!} + 2 \ln B - 1.7816}{\Omega_0^3 B^2},$$

and use has been made of the relations (again considering only f_0):

$$\langle \theta^2 \rangle = X(1 - X/6),$$
$$\langle \theta^4 \rangle = 2X^2. \tag{6}$$

τ_1 and τ_2 are slowly varying functions of B, which can be easily tabulated with great accuracy.

Up to this point the main differences between the present method of evaluating the PLC correction and the one developed in ref. [8] are the omission of the term originating from f_1 and the different integration of the term f_0 which is performed here completely analytically, without the approximations of ref. [8] which cause it to break down for low values of B.

A simple but accurate inversion algorithm to compute t starting from a given value of $\langle s \rangle$, which is necessary whenever a boundary crossing occurs, can be derived from eq. (5) by expanding it and solving for t. Such inversion leads to a maximum error on the computed $\langle s \rangle$ to t relation, which is always $< 1\%$ of the PLC computed directly and usually much better. Since the PLC correction itself resulting from that equation is always smaller than 20%, provided that $\chi_r < 1$, the accuracy of the inversion algorithm is surely much better than the intrinsic error due to the several approximations used.

In most usual multiple scattering algorithms (e.g. the standard EGS4 one) an average PLC correction together with the end step scattering angle are the only quantities needed to perform a step. In more sophisticated algorithms a lateral displacement algorithm (LDA) is also applied to allow the use of larger steps. The one adopted in ref. [8], which is slightly modified from that originally proposed by Berger [15], makes use of the relation

$$r = \langle s \rangle \sin \theta/2,$$

where r is the radial displacement, whilst the longitudinal displacement is given simply by $\langle s \rangle$. In that way, however, the longitudinal displacement always results in the same value corresponding to the average $\langle s \rangle$, for a given curved step length t, whilst the radial displacement is fully correlated to the final scattering angle θ. If we project the step onto a plane containing the axis of the original motion, the possible final points

are distributed on a line perpendicular to the z-axis, in such a way that a larger θ correspond to a larger total straight path length (p in our notation). This is in some way nonphysical (on the average we can expect that particles undergoing larger deflections will experience smaller straight steps). In the next section a simple model is developed for correlating not only the radial displacement but also the longitudinal one to the deflection angle, so as to try to overcome these problems. Before deriving such an expression we need an approximate estimation not only of $\langle s \rangle$ but also of the variance of s which will be employed together with the angular correlations developed below to completely define our model. The expression we start from is

$$s^2 = 2\int_0^t \mathrm{d}t' \cos\theta(t') \int_0^{t'} \mathrm{d}t'' \cos\theta(t'').$$

The main problem is to develop a simple but accurate approximation for the innermost integral; we finally adopted a trapezoidal approximation applied to the integral after rearranging the integration variable. We can write

$$\int_0^{t'} \mathrm{d}t'' \cos\theta(t'') = \int_0^{\langle s(t') \rangle} \frac{d\langle s'' \rangle \cos\theta''}{\langle \cos\theta'' \rangle} \approx \frac{\langle s' \rangle}{2}\left(1 + \frac{\cos\theta'}{\langle \cos\theta' \rangle}\right). \tag{7}$$

This way of approximating the innermost integral should be more accurate than the straightforward approximation

$$\int_0^{t'} \mathrm{d}t'' \cos\theta(t'') \approx \frac{t'}{2}(1 + \cos\theta'). \tag{8}$$

The expression derived in the following shows that the approximation of eq. (7) leads to a definite positive σ_s^2, while the simplest expression (8) does not. After some standard algebra we get

$$s^2 = 2\int_0^t \mathrm{d}t' \langle s' \rangle \cos\theta' + \int_0^t \mathrm{d}t' \langle s' \rangle \frac{\cos^2\theta' - \cos\theta' \langle \cos\theta' \rangle}{\langle \cos\theta' \rangle}.$$

Averaging the above expression leads to the final result

$$\sigma_s^2 = \langle s^2 \rangle - \langle s \rangle^2 = \int_0^t \mathrm{d}t' \langle s' \rangle \frac{\langle \cos^2\theta' \rangle - \langle \cos\theta' \rangle^2}{\langle \cos\theta' \rangle}.$$

Note that no explicit expression for the distribution has been used up to now. Expanding as usual up to θ^4 and solving by considering only the f_0 contribution, it can be shown that

$$\sigma_s^2 = \frac{t^2}{4}\tau_3(B)X^2, \tag{9}$$

where $\tau_3(B)$ is given by

$$\tau_3(B) = 1 + \frac{1}{2B} - \frac{4\sum_{k=1}^{\infty} \frac{(4B)^k}{kk!} + 4\ln B + 6.9608}{\Omega_0^4 B^3}.$$

Again τ_3 is a slowly varying function of B which can be easily tabulated.

3.4. Angle selection

The angle θ is, obviously, selected from the distribution given in eq. (3), that is, the Molière distribution including the f_1 and f_2 terms and corrected according to Bethe.

We adopt a simple choice to select the angle η: it is taken equal to the previously selected angle θ times the ratio ρ between the average values of η and of θ. ρ is given by

$$\rho = \frac{1}{\sqrt{3}}\sqrt{\frac{B^*}{B}}\,\frac{1 + 0.982/B^* + 0.117/B^{*2}}{(1 + 0.982)/B + 0.117/B^2}, \tag{10}$$

where we have neglected the Bethe correction when averaging. In this way the correct average value for η is assured a priori, and, providing we neglect the small difference between B^* and B, the resulting distribution for η corresponds to the theoretical one. A proper correlation coefficient between the angles Ψ and Φ can be achieved with a suitable selection of the angle $\Delta\omega$. Our choice for $\Delta\omega$ results in a correlation coefficient between Ψ and Φ that for large B and small angles tends to the one given by the simple Gaussian theory [16], $\sqrt{3}/2$, while for small steps it is closer to unity. It is given (somewhat arbitrarily) by

$$\cos\Delta\omega = \frac{1}{2\rho}. \tag{11}$$

It is in fact straightforward to show that, with the assumption described above, the following holds (note that $\langle\Psi\rangle, \langle\Phi\rangle = 0$):

$$(\mathrm{corr}(\Psi\Phi))^2 = \frac{\langle\Psi\Phi\rangle^2}{\langle\Psi^2\rangle\langle\Phi^2\rangle} = \cos\Delta\omega.$$

Finally, to complete the angular selection, the sign of $\sin\Delta\omega$ and the angle ϕ are chosen randomly.

3.5. Step length selection

A step can be performed once the direction and the length of the particle displacement, that is η, ω and p, are given. The sampling schemes for all angular quantities have been defined. Any suitable selection scheme for p or s, which are linked by $s = p\cos\eta$, must fulfill the expressions derived in the previous sections for $\langle s \rangle$ and σ_s^2 (eqs. (5) and (9)). These requirements call for

expressions for s or p which depend on the sampled angles. A simple approximation for s can be expressed as

$$s = s_{\text{corr}} \cos\theta + s_{\text{uncorr}}, \tag{12}$$

where s_{corr} and s_{uncorr} are unknown coefficients expressing the fraction of s correlated and uncorrelated, respectively, with the final deflection angle θ. They should be computed according to the expressions for $\langle s\rangle$ and σ_s^2. Eq. (12) and the analogue one for p,

$$p = p_{\text{corr}} \cos\kappa + p_{\text{uncorr}}, \tag{13}$$

are obvious first order approximations which can be easily understood looking at the integral or differential expressions for s and p

$$s = \int_0^t \mathrm{d}t' \cos\theta(t'), \qquad \Delta s = \cos\theta\, \Delta t,$$

$$p = \int_0^t \mathrm{d}t' \cos\kappa(t'), \qquad \Delta p = \cos\kappa\, \Delta t,$$

where we recall that κ is the angle between the position and velocity vectors and is related to η, θ and $\Delta\omega$ by eq. (1). Eqs. (12) and (13) can be regarded as generalizations of the approximation derived for s by Berger [15]. A straightforward possibility could be to determine s_{corr} and s_{uncorr} using eqs. (5) and (9); p can then be computed by dividing by $\cos\eta$. Even though this scheme would be consistent with our derivation, an equivalent approach where p is directly selected has been preferred since it has a few advantages. In fact p is the quantity actually needed in a real calculation, and computing it directly avoids the problem of the alternative approach when η approaches $\pi/2$ and makes it easier to check the fulfillment of physical conditions like $p \le t$. Furthermore, since the wiggliness correction is of course much smaller when computed with respect to p instead of s, the effect of all our approximations is minimized. Eqs. (5) and (9) for $\langle s\rangle$ and σ_s^2 can still be used to compute p_{corr} and p_{uncorr}. Taking into account the relations among the various angles and s and p, the following holds:

$$\begin{aligned}
\langle s\rangle &= p_{\text{corr}}\langle\cos\kappa\cos\eta\rangle + p_{\text{uncorr}}\langle\cos\eta\rangle,\\
\sigma_s^2 &= p_{\text{corr}}^2\left(\langle\cos^2\kappa\cos^2\eta\rangle - \langle\cos\kappa\cos\eta\rangle^2\right)\\
&\quad + p_{\text{uncorr}}^2\left(\langle\cos^2\eta\rangle - \langle\cos\eta\rangle^2\right)\\
&\quad + 2p_{\text{corr}}p_{\text{uncorr}}\left(\langle\cos\kappa\cos^2\eta\rangle\right.\\
&\quad \left. - \langle\cos\kappa\cos\eta\rangle\langle\cos\eta\rangle\right).
\end{aligned} \tag{14}$$

Let us expand p_{corr} and p_{uncorr} in powers of X:

$$p_{\text{corr}} = t\left(p_{0c} + p_{1c}X + p_{2c}X^2\right),$$

$$p_{\text{uncorr}} = t\left(p_{0u} + p_{1u}X + p_{2u}X^2\right).$$

Expanding also all angles up to θ^4 (recall that $\eta = \rho\theta$), and using the results for $\langle\theta^2\rangle$ and $\langle\theta^4\rangle$ presented in section 3.3, it is possible to evaluate all the averages in eq. (14) and, after comparing with the expressions for $\langle s\rangle$ and σ_s^2 (eqs. (5) and (9)) to determine the coefficients $p_x s$. It is important to remark that, whilst p_{0c} and p_{0u} are completely determined, there is some degree of freedom in the choice of p_{1c}, p_{1u}, p_{2c} and p_{2u}, since the equation for σ_s^2 has only terms of order X^2 and therefore gives information only concerning p_{0c} and p_{0u}. We adopted the simple but questionable prescription of choosing $p_{1c}, p_{2c} = 0$: anyway we do not believe this choice to be critical.

Since the algebra is straightforward but very tedious we quote here only the final result for the adopted expressions for the p_x coefficients:

$$\begin{aligned}
&p_{0c} = \tfrac{17}{43} - U, \qquad p_{0u} = \tfrac{26}{43} + U,\\
&p_{1c} = 0, \qquad\qquad p_{2c} = 0,\\
&p_{1u} = \tfrac{30}{43}\rho^2 - \tfrac{1}{2}\rho^2 U - \tfrac{1}{2}\tau_1(B),\\
&p_{2u} = \tfrac{17}{516} - \tfrac{32}{129}\rho^2 + \tfrac{3}{86}\rho^4 - U\left(\tfrac{1}{12} - \tfrac{5}{12}\rho^2 - \tfrac{1}{3}\rho^4\right)\\
&\qquad - \tfrac{1}{4}\rho^2\tau_1(B) + \tfrac{1}{6}\tau_2(B),
\end{aligned} \tag{15}$$

where

$$U = \sqrt{129\tau_3(B) + 160\rho^4}\,/\left(43\rho^2\right).$$

It is interesting to point out how the approximation that was made in neglecting the f_1 contribution when deriving eqs. (5) and (9) is actually partially compensated by this algorithm. In fact, the expression for the modulus of the position vector p which has been obtained here is based on the Gaussian approximation: that is, if one sampled the angles θ and η only from the Gaussian part of the distribution, one would obtain a mean value and a variance for s equal to those given by eqs. (5) and (9). However, it must be remembered that we do not neglect f_1 and f_2 in the angular sampling, so their contribution comes partially back through the correlated part of p and through the value of $\cos(\rho\theta)$. In fact this "automatic" compensation is believed to be one of the reasons for the satisfactory results of FLUKA presented in section 6.

3.6. Corrections to the Molière single scattering cross section

At the basis of the Molière multiple scattering theory there is the assumption that the single scattering law can be described using an expression that contains the screening correction to the Rutherford formula:

$$\frac{\mathrm{d}\sigma_{\text{mol}}}{\mathrm{d}\Omega} = \left[\frac{z^2Z^2e^4}{4c^4\beta^2E^2\sin^4\frac{1}{2}\theta}\right]\left[\frac{(1-\cos\theta)^2}{\left(1-\cos\theta+\frac{1}{2}\chi_a^2\right)^2}\right], \tag{16}$$

which in the small angle approximation becomes

$$\frac{d\sigma_{small}}{d\Omega_{small}} = \left[\frac{4z^2Z^2e^4}{c^4\beta^2E^2\theta^4}\right]\left[\frac{\theta^4}{\left(\theta^2+\chi_a^2\right)^2}\right],$$

$(d\Omega_{small} = 2\pi\theta\, d\theta)$.

The approximate expression for the screening angle χ_a as computed by Molière is

$$\chi_a^2 = \frac{\chi_{cc}^2\, e^{1-2\gamma}}{b_c E^2\beta^2}, \qquad \gamma = 0.577\cdots.$$

This expression does not contain the so-called spin-relativistic correction coming from the Mott formula. It is possible that some problems such as backscattering can be affected by this approximation.

Another effect, which is important mainly at high energies for e^+, e^- but already at medium energies for massive particles, is the scattering suppression due to the nuclear finite size, usually described through a nuclear charge form factor F_n which modifies the single scattering cross section.

The method adopted here to take into account these corrections stems from two observations: the first is that these corrections tend to vanish at small scattering angles, the second is that the relative importance of the single scattering tail (the f_1/B term) grows at large angles. One is therefore encouraged to try to apply the correction only to the single scattering distribution. Of course, this approach will bring some limitations in the range of applicability of the whole algorithm, as will be described later.

Let us decompose the multiple Molière scattering distribution as corrected by Bethe into two contributions, the first one being the contribution from single scattering:

$$2\pi f_{mol}(\theta_r, B)\sqrt{\sin\theta/\theta}\,\theta\, d\theta$$
$$= 2\pi\left[f_{single} + \left(f_{mol} - f_{single}\right)\right]\sqrt{\sin\theta/\theta}\,\theta\, d\theta. \quad (17)$$

Using the small angle approximation and recalling the definition of χ_c, it is easy to show that in the Molière derivation the following holds:

$$2\pi f_{single} = \frac{2\chi_c^2}{\left(\theta^2+\chi_a^2\right)^2}. \quad (18)$$

Let us now define

$$K_{corr}(\theta) = \frac{d\sigma(\theta)}{d\Omega} \Big/ \frac{d\sigma_{small}(\theta)}{d\Omega_{small}}, \quad (19)$$

where $d\sigma/d\Omega$ is the actual cross section for single scattering, and

$$r_{single}(\theta, B) = f_{single}(\theta, B)/f_{mol}(\theta, B),$$

$$K_{Bethe}(\theta) = \sqrt{\sin\theta/\theta}.$$

Now, multiplying the single scattering part of eq. (17) for the correction factor K_{corr}, one obtains a corrected distribution for θ given by

$$P_{corr}(\theta, B)\, d\theta = 2\pi\theta f_{mol}(\theta_r, B)K_{mod}\, d\theta_r,$$
$$K_{mod}(\theta, B) = \left[1 - r_{single}(\theta, B)\right]K_{Bethe}(\theta) + r_{single}(\theta, B)K_{corr}(\theta). \quad (20)$$

An implicit assumption is that the Molière screening correction must be valid at small angles, a requirement which is usually well satisfied, as demonstrated in refs. [17,14]. The substitution of eq. (20) is meaningful only if it holds that corrections are negligible for all component of the multiple scattering distribution but the single scattering one. In other words, the angle θ_{start} at which the correction factor K_{corr} starts to differ significantly from unity must be large compared to the characteristic angle of the multiple scattering distribution, which is given by $\chi_r = \chi_c\sqrt{B}$. This requirement translates into

$$\theta_{start} = f\chi_r, \qquad f \gg 1 \quad (21)$$

(typical values used in FLUKA for f are in the range 2–5). From this condition one obtains a constraint for t_{max}, which is given by

$$B_{max} = 2\ln\left(\frac{E\beta b_c^{1/2}\theta_{start}}{f\chi_{cc}}\right),$$
$$t_{max} = \frac{\beta^2\exp B_{max}}{b_c B_{max}}. \quad (22)$$

A practical algorithm could be to choose θ_{start} as the angle where the correction for the single scattering cross section is suitably small, $K_{corr}(\theta_{start}) = 1 \pm \epsilon$, $\epsilon \ll 1$, and to utilize the most stringent constraint for t_{max} between the condition of eq. (22) and the Bethe one, $\chi_r \lesssim 1$. The angular deflection can still be sampled from the Molière distribution and a rejection can be applied according to

$$f_{reje}(\theta, B) = K_{mod}(\theta, B)/K_{mod}(\theta_{max}, B), \quad (23)$$

where θ_{max} is the angle at which the factor K_{mod} takes its maximum value.

3.7. Summary

We developed a model in which not only the average value of the PLC, but also its variance are accounted for within our approximations, thanks to the selection method for p explained in section 3.5. Furthermore, the position angles η and $\Delta\omega$ are chosen in such a way as to obtain the correct average value and roughly also the correct distribution for η, with a proper correlation between the projected position and direction angles.

Of course, a further refinement could be represented by deriving proper θ-dependent distributions for η and $\Delta\omega$ instead of the simple approximations outlined above. However, such distributions cannot be easily computed and we feel it is likely that our assumptions are already appropriate to better sample phase space in comparison with previously developed models.

4. Main features of the FLUKA code

FLUKA [1] is a Monte Carlo code designed principally for studying the interaction of high energy beams of hadrons or leptons with matter. The code has been greatly improved and enlarged in the past few years, mainly to allow it to cope with problems related to the new CERN accelerators (LEP and the design studies for the LHC project). The code is interfaced with the CG combinatorial geometry package which allows the use of complex 3D geometries.

Previous versions of FLUKA made use of EGS4 to follow the electromagnetic component [18]. The present version of the code retains only a small fraction of the original EGS4 coding. Only Bhabha and Möller scattering and positron annihilation in flight are still handled by the original routines. The treatment of all other physical processes is completely new (e^-, e^+ transport, bremsstrahlung, photoelectric effect) or greatly changed (Compton scattering and pair production): details of these modifications are given elsewhere [1].

The model outlined in section 3 has been fully implemented for all charged particles transported by the code. Any energy dependent quantities that are calculated during the history generation, are evaluated at the average energy of the step. The energy variation along the step for quantities which can be computed before the history generation is calculated in an accurate fashion by means of integration. The user can control the step length through two different mechanisms: by setting a maximum fractional energy loss per step for each material (from this point referred to as ΔE_{step}), and by setting a maximum geometrical step length for each region. The first condition is checked by the code together with possible path length restrictions arising from spin relativistic and/or nuclear form factor corrections (see above) so as to compute the maximum allowed path length $t_{\max}$. The variation with energy both of the discrete event cross sections and of the collision stopping power has been fully taken into account in the coding.

An optional spin-relativistic correction is implemented according to the second Born approximation formula (for spin-$\frac{1}{2}$ particles):

$$\frac{d\sigma}{d\Omega} = \frac{d\sigma_{\text{mol}}}{d\Omega}\left[1 - \beta^2 \sin^2\tfrac{1}{2}\theta - \pi z Z \alpha\beta \sin\tfrac{1}{2}\theta\left(1 - \sin\tfrac{1}{2}\theta\right)\right],$$

where z is the particle charge with its sign.

Optional simple nuclear form factors are implemented, and easy hooks for more complex ones as well as for changing the default spin-relativistic correction are provided through special routines.

5. Implementation of the new model in MCNPE-BO

MCNPE-BO [19] is a Monte Carlo code for the coupled transport of neutrons, photons and electrons developed at ENEA, Bologna, in order to have a powerful and user-oriented code in the low–medium-energy range (roughly from 10 keV up to 100 MeV), principally for radiation protection and dosimetry.

The layout of the transport process for all tracked particles neutrons, photons and electrons is based on the original MCNP-3a [20] structure, although for the electron physics it uses the relevant EGS4 routines. The multiscattering model previously described has been implemented in MCNPE-BO without the correlation algorithm for the angles. This actually overestimates the resulting angular dispersion which probably explains the slightly different behaviour between MCNPE-BO and FLUKA, highlighted by the results of the benchmarks later reported. This difference could of course be reduced by shortening the step length.

The maximum value of the step length is set by the user as some fraction of the total range of the electron.

The presence of a refined algorithm for the boundary crossing allows a satisfactory treatment of interface problems [19].

The continuous energy variation along the step is taken into account: our aim is to have at every stage of the calculation an exact value of all energy-dependent parameters averaged on the curved path.

Neither spin-relativistic nor nuclear form factor corrections have been implemented so far.

6. Benchmarks

Some benchmarks of both codes are presented in the following to demonstrate the validity of the described algorithms.

6.1. FLUKA benchmarks

Obviously, we were interested in those tests which could best verify the achievement of our initial goals.

The new PLC correction should assure stability of results against variations of the step size, at least at the energies of interest for FLUKA users. Moreover, the refined treatment of deflections and boundary conditions should allow to simulate problems involving interfaces between different media as well as reflections and angular distributions of scattered particles.

All experimental data have been chosen from standard benchmarks (mostly taken from those described in ref. [21]); unfortunately, none of them involves hadrons or charged particles other than electrons, mainly because it is difficult to find an experiment strongly sensitive to multiple scattering.

CPU times are given using standard Vax accounting unit (VAX 11/780 = 1), even though runs were actually performed on a variety of Vax-station models running VMS 5.4-1A, with performances ranging from 3 to 7 times that unit. Care must be taken in considering the absolute timing performances reported below because of two factors which somewhat slow down the code in these kind of calculations. The first is that all the code runs under double precision, since this is mandatory for all high energy problems; of course this results roughly in an extra factor of 2 when comparing with a code partially or completely running under single precision. The second is related to the structure of the code: since it must be able to transport a variety of particles in complex geometry, a non-negligible amount of time is spent inside routines which act merely as interfaces. Finally the step size dependence of the CPU time is partially hidden for benchmarks 1, 3 and 4 by the use of region-dependent cutoffs. Concerning timing, this makes really sensitive to the step size only that fraction of source electrons hitting the target near the central axis.

6.1.1. Energy deposition profiles (benchmarks 1 and 2)

Step-size stability for depth–dose curves has been tested under two conditions. The first refers to the data contained in ref. [22], where the depth–dose profiles produced by 20 MeV electrons in water have been measured (this benchmark will again be used in interface problems, see next section).

Calculations have been performed transporting electrons coming from a point source situated at 100 cm from a water barrel with a radius of 5 cm and a depth of 21 cm, as in ref. [22]. The difference between calculated on-axis dose with the fractional energy loss per step, ΔE_{step} set at 5% and 20% stays within $\pm 5\%$ (as plotted in fig. 1) except at the end of the range, where, however, the dominating effect is statistical. The data in fig. 1 are relative to runs of 200 000 electrons each (CPU time: 0.4 s per electron at 20%, 0.5 s at 5%), and have statistical errors which range from 1% to 3% at depths greater than about 9 cm and increase rapidly towards the end of the electron range.

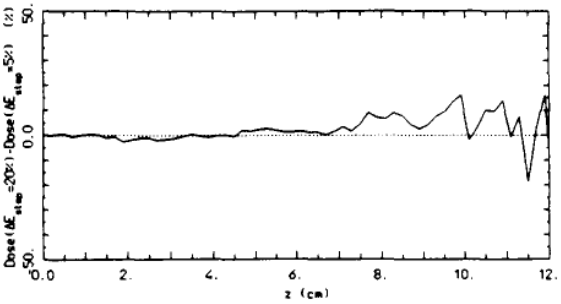

Fig. 1. Difference in percentage between calculations performed with FLUKA using a fractional energy loss per step, ΔE_{step} set at 20% and 5% for a 20 MeV broad electron beam incident on a homogeneous water phantom (see the text and ref. [22] for further details).

The agreement with experimental data is satisfactory, as can be seen in fig. 2 (here the calculated curve corresponds to 800 000 electrons).

Another test has been performed making a comparison with measurements of depth–dose curves due to a broad beam of 500 keV electrons on aluminium [21]. The target was an aluminium slab 0.1 cm thick and of very large lateral dimensions. Results computed for a pencil beam have been converted to broad beam depth–dose curves using standard relations. This allowed to get quite good statistics within a reasonable computer time. The curves obtained with the fractional energy loss per step, ΔE_{step}, set at 20, 8 and 2% are compared with the experimental data in fig. 3. The curves show a good agreement with data and among themselves (CPU time: 0.27 s per electron at 20%, 0.46 s at 8% and 1.4 s at 2% – source particles 50 000).

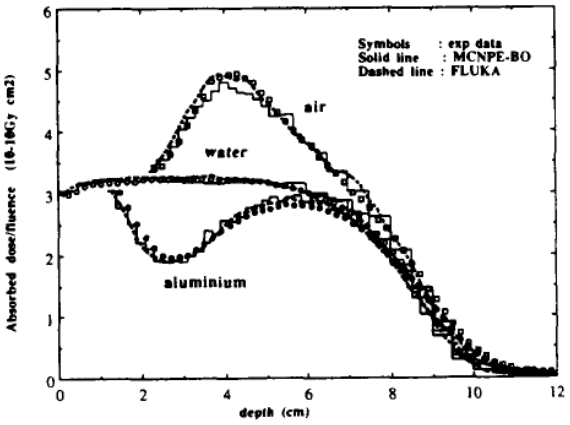

Fig. 2. Comparison of calculated and experimental depth–dose profiles, obtained with 20 MeV electrons incident on a water phantom, in the homogeneous case and with Al or air inhomogeneities. Experimental data are from ref. [22]. All values are given per unit incident fluence.

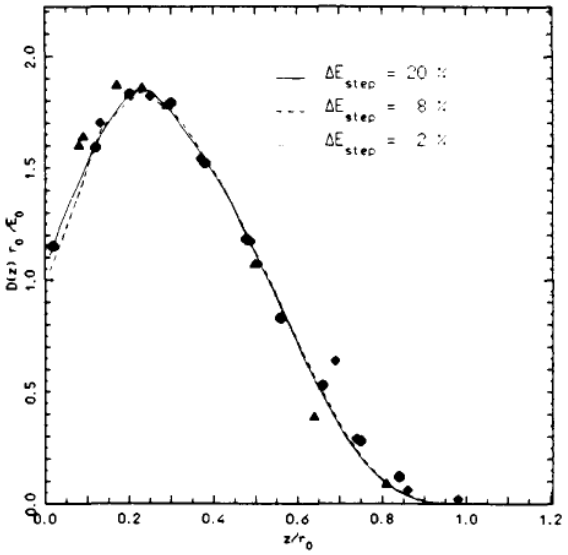

Fig. 3. Comparison of calculated (FLUKA) and experimental depth–dose profiles, for 0.5 MeV electrons incident on Al, with three different step sizes. Symbols refer to three sets of experimental data [21]. The normalization of the data is the same as in ref. [21]. r_0 is the csda range as assumed in ref. [21].

6.1.2. Inhomogeneities (benchmarks 3 and 4)

The same electron beam and water phantom of the first benchmark are found in the simulations performed to obtain the longitudinal and radial dose profiles in two "standard" nonhomogeneous conditions, as described in ref. [22]: a small cylinder of air (1.0 cm diameter, 2.0 cm length) or aluminium (1.0 cm diameter, 1.0 cm length), has been introduced into the water phantom at a depth of 2 mm on the beam axis. The resulting longitudinal dose profiles (computed with a fractional energy loss per step, ΔE_{step}, set at 10%) are shown in fig. 2, and show good agreement with the measured ones (CPU time: 0.58 s per electron for both inhomogeneities – source particles: 800 000). Radial profiles computed at various depths behind the cylindrical inhomogeneities are compared in figs. 4 and 5 with the experimental data. They are more sensitive to statistics, especially in the innermost bins, where some departure from experiment does occur, but this stays within a few percent. The slight discrepancies for the largest depths can be explained by a small difference between the configuration used in the simulation and the experimental one (see ref. [22] for details).

6.1.3. Angular distributions (benchmarks 5 and 6)

Angular distributions of electrons transmitted by or reflected from Al and Cu foils have been compared with experimental results [23,24]. The transmission and reflection of 1.75 MeV electrons perpendicularly incident on a 0.364 g/cm^2 Cu foil, and of 1 MeV electrons transmitted through Al foils of thickness 0.1, 0.22 and 0.32 g/cm^2 have been simulated. The fractional energy loss per step, ΔE_{step}, ranged from 4 to 10%. Results are shown graphically in figs. 6 and 7 (CPU time: from 0.12 to 0.38 s per electron for the Al foils, depending on the thickness, 0.14 s for the Cu foil – source particles: 200 000). The percentage of transmitted electrons through the Al foils can be found in table 1.

The agreement with experiments is very good, except for electrons reflected near 180° from the Cu foil, and the transmitted electrons through the Al foil of intermediate thickness, where we have a difference of about 10% from the experimental data at small angles.

6.1.4. Thin foil energy spectra (benchmark 7)

We show in fig. 8 the energy spectra of electrons transmitted through the Al foils mentioned in the

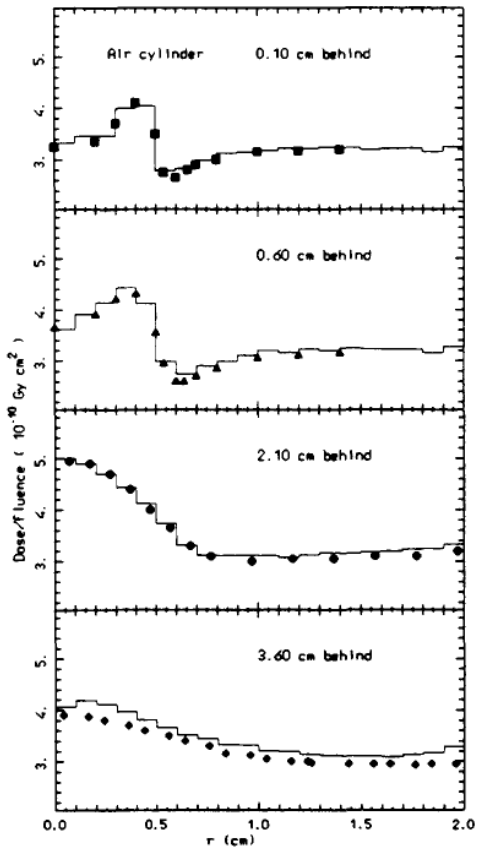

Fig. 4. Radial dose profiles for 20 MeV electrons incident on the water phantom of fig. 2 with a cylindrical air inhomogeneity (see the text and ref. [22] for further details). Symbols are experimental data [22], the histograms are FLUKA results. Quoted depth refers to the distance from the end of the inhomogeneity.

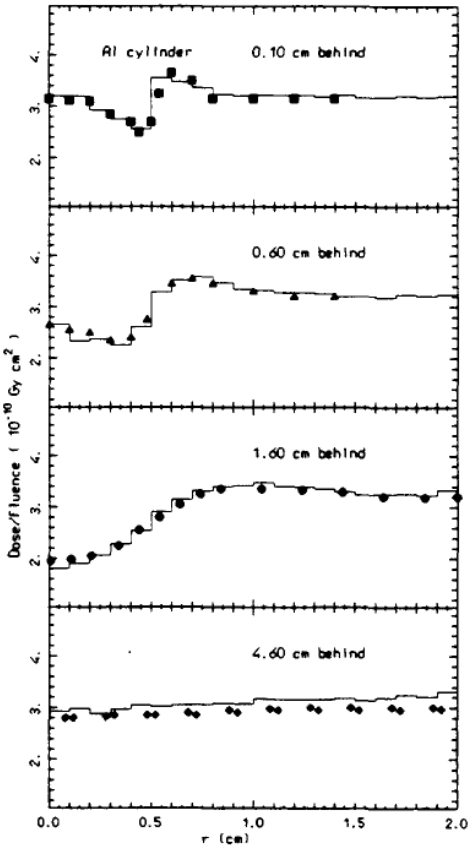

Fig. 5. As in fig. 4 but for a cylindrical Al inhomogeneity.

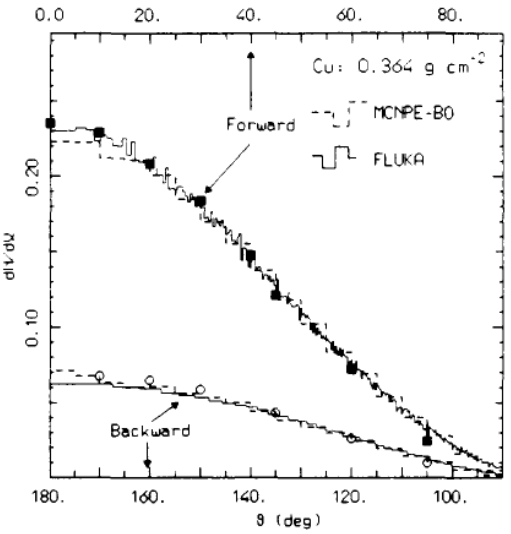

Fig. 6. Angular distributions of electrons transmitted through or reflected from a Cu (0.364 g/cm^2) foil. The incident energy is 1.75 MeV, and only electrons emerging with energy ≥ 150 keV are included. Solid histograms are FLUKA results, dashed ones MCNPE-BO results. Symbols are experimental data from ref. [24], normalized to the calculated integral of transmitted or reflected electrons, respectively as computed by FLUKA.

previous section. Here we expected some problems because the code does not include Landau fluctuations of the energy loss. In the limit of very thin foils this results in an energy spectrum for transmitted electrons which has the shape of a δ-function. For thicker foils the effect is that of a sudden fall of the spectrum in the high energy part, as can be seen in fig. 8 in the curve relative to the 0.10 g/cm^2. We tried to partially account for this by lowering the threshold for discrete events (bremsstrahlung and Möller scattering) down to 5 keV. This allowed the experimental data for the 0.32 and 0.22 g/cm^2 foils to be reproduced in a satisfactory way.

6.1.5. Backscattering (benchmarks 8 and 9)

Since the Molière theory is based on the small angle approximation, its validity when applied to backscattering problems should be demonstrated. In the following it will be shown that the proposed algorithm when properly applied (and possibly corrected for spin-relativistic effects) produces results of the same quality as those produced by codes based on the Goudsmit and Saunderson formalism.

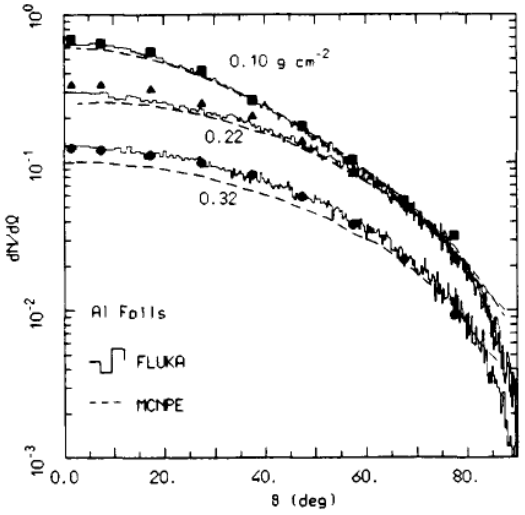

Fig. 7. Angular distributions of electrons transmitted by Al foils of different thicknesses. Initial energy is 1 MeV, outgoing electrons are included down to 100 keV. Solid histograms are FLUKA results, dashed lines are MCNPE-BO results. Symbols are experimental data from ref. [23].

Table 1
Fraction of electrons with initial energy 1 MeV and outgoing energy ≥ 100 keV transmitted from Al foils of thickness z; experimental data are from ref. [23]. Errors on exp. data are about 5%, in the calculations less than 1%

	z [g/cm^2]		
	0.1	0.22	0.32
Exp.	0.98	0.69	0.27
FLUKA	0.95	0.63	0.28

A comparison with EGS4 will also be presented, since there are no published results of that code in this field. This comparison has been carried out using EGS4 as implemented in the FLUKA87 code [18]. This allowed us to use the same input cards and data, geometry and scoring routines used also for FLUKA. In fig. 9 the results obtained with FLUKA, EGS4 (as installed in FLUKA87) and MCNPE-BO for the number reflection coefficient from aluminium foils of saturation thickness are presented and compared with available experimental data. The calculated data include all electrons with energy ≥ 1 keV. The foils have been split into three longitudinal sections with increasing cutoff energies for electron transport and production. The effect of the step size on the computed backscattering coefficient has been investigated both for FLUKA and EGS4: it must be pointed out that in the first (very thin) foil layer, where the cutoff energy was forcibly set to 1 keV, step lengths were dominated by the mean free path between subsequent δ-ray production events rather than by the input step size. The dashed area in fig. 9 shows the variation of the results computed with FLUKA allowing the fractional energy loss per step, ΔE_{step}, to range from 20 to 5% (further

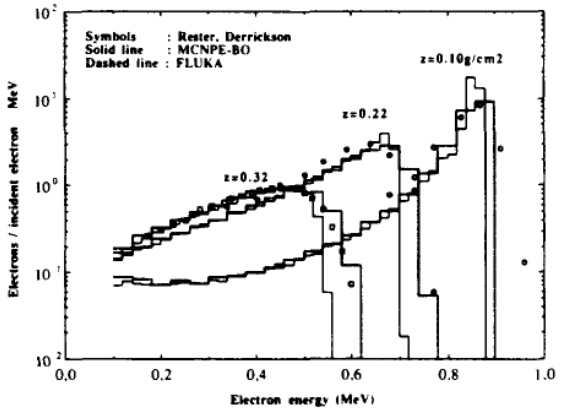

Fig. 8. Energy spectra of transmitted electrons, for the same configurations as in fig. 7. Dashed histograms are FLUKA results, solid histograms are MCNPE-BO results. Symbols are experimental data from ref. [23].

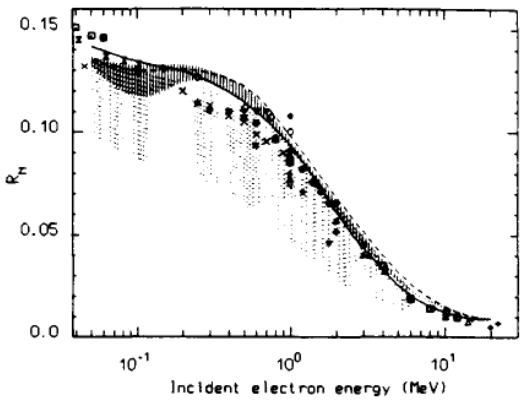

Fig. 9. Number reflection coefficient R_N for electrons incident perpendicularly on aluminium foils of saturation thickness. Symbols: experimental results. Solid line: FLUKA results with spin-relativistic corrections. Dashed line: MCNPE-BO results. Dashed and dotted areas: results for different step length constraints for FLUKA and EGS4, respectively (see text for further details and references).

reductions produce results indistinguishable from the $\Delta E_{step} = 5\%$ ones), the highest values corresponding to the smallest ΔE_{step}. The dotted area has the same meaning for EGS4, where now ΔE_{step} has been set as small as 1%. Despite this very small value, results are still very sensitive to the chosen step length (there is a typical 10–15% difference between results computed with $\Delta E_{step} = 2\%$ and 1%): shorter steps cannot be used without switching off the EGS4 multiple scattering algorithm (it occurred already for 11% of the steps at 50 keV with $\Delta E_{step} = 1\%$). The solid line has been computed with FLUKA including also spin-relativistic corrections as described in section 3.5 ($\Delta E_{step} = 8\%$) which produces a small but clearly distinguishable improvement in the results. The agreement of this set of data with the experiments is noteworthy, and also remarkable is the low sensitivity of the FLUKA results to the adopted step length (12% at maximum at 100 keV), taking into account that backscattering should be extremely sensitive to these kind of artefacts. As expected, EGS4 exhibits a much stronger variation and meaningful results could be obtained only by pushing step lengths to the shortest allowed values. It is quite interesting to compare the timing performances: it is worthwhile to recall that the geometry, scoring and all parts of the codes but the relevant electron transport routines are exactly the same in FLUKA and EGS4 (as implemented in FLUKA87) runs, so comparisons are fully meaningful. The elapsed CPU time per primary electron at 50 keV was 0.91 s for EGS4 ($\Delta E_{step} = 1\%$, it is not reported for other values since they do not produce meaningful results) and 0.17, 0.29 and 0.26 s for FLUKA at $\Delta E_{step} = 20\%$, 5% and with the spin-

relativistic corrections, respectively. At 1 MeV the elapsed time was 1.2 s for EGS4 and 0.32, 0.51 and 0.53 s for FLUKA, at 6 MeV 2.5 s for EGS4 and 0.67, 1.1 and 1.3 s for FLUKA. The number of source particles ranged from 100 000 for the lowest energies to 50 000 for the highest ones: the resulting statistical errors on the computed backscattering coefficient range from a few tenths of a percent at 50 keV up to 1–2% at 20 MeV. References for the experimental data shown in fig. 9 at $E \geqslant 200$ keV can be found in ref. [25], whilst at the lowest energies they have been obtained from refs. [26–29].

A similar comparison has been carried out for gold as an example of a heavy material. The results obtained by FLUKA and EGS4 at three different energies are compared between themselves and with the experimental data in table 2. Calculations have been performed in a similar fashion as for the aluminium case. FLUKA results have been computed with the spin-relativistic correction and $\Delta E_{step} = 8\%$. For EGS4 runs $\Delta E_{step} = 1\%$ has been used even though this caused the multiscattering algorithm to turn off for a significant fraction of the steps (30% at 100 keV, 12% at 3 MeV). Larger values resulted in very inaccurate results whilst smaller ones virtually inhibit the scattering of low energy electrons. The agreement of FLUKA results with the experimental data is satisfactory, also taking into account that the simplified spin-relativistic correction used here is poor for gold. There is evidence that EGS4 cannot converge to the right answer before steps are so short that they turn off the multiscattering algorithm: this is in agreement with the remarks of refs. [8,12] about EGS4 behaviour with heavy elements. It is worthwhile to point out that timing differences are quite large at low energies, while they tend to vanish at the highest energy.

6.2. MCNPE-BO benchmarks

A full description of the benchmarks is given in a previous section referring to FLUKA. Note in the following, CPU times refer to IBM-3090/300E, op. sys. MVS/SP JES 2.2.0.

6.2.1. Benchmark 1

The agreement of the MCNPE-BO results (see fig. 2) with experimental data is excellent; the CPU time per electron was 0.014 s and the errors less than 1.5% for 500 000 source particles. The fraction of the total range, used to determine the maximum step length, could arrive without problem up to the value 0.25. This is because the cell dimensions were relatively large. However, it should be noted that at the beginning of the water slab where electrons have lost little energy it is the distance to the cell boundary which fixes the actual step length, rather than the dimension of the step length defined by the user.

6.2.2. Benchmark 3

The comparison (see fig. 2) was performed for the longitudinal profile. In order to achieve a detailed dose profile we employed very small cells; to obtain a reasonable result, the maximum step length had to be not larger than 0.1 of the total range. The CPU time per electron was 0.0036 s, although we had to run 4000 000 source particles to obtain an error less than 1.5%. Care

Table 2
Number reflection coefficient for gold foils of saturation thickness

Electron energy [MeV]	Exp. data	FLUKA		EGS4	
		Result	CPU [s]	Result	CPU [s]
0.1	0.49 [a]	0.488 ± 0.002	0.41	0.475 ± 0.003	3.8
	0.513 [b]				
1	0.43 [c]	0.440 ± 0.003	1.9	0.391 ± 0.002	3.3
	0.45 [a]				
	0.46 [d]				
	0.47 [e]				
	0.51 ± 0.04 [f]				
3	0.31 [c]	0.314 ± 0.002	3.1	0.270 ± 0.002	2.8
	0.302 ± 0.021 [g]				

[a] Ref. [26].
[b] Ref. [28]: value measured at 102 keV.
[c] Ref. [33].
[d] Ref. [31].
[e] Ref. [32].
[f] Ref. [30].
[g] Ref. [34]: value measured at 3.24 MeV, it should be increased roughly by 0.08 to scale it at 3 MeV.

must be taken when considering these values, since variance reduction techniques have been extensively used to reduce computer time.

6.2.3. Benchmarks 5 and 6

The angular distribution (see fig. 7) was calculated for electrons transmitted through the aluminium foils of thickness 0.1, 0.22 and 0.32 g/cm^2. The values for the first foil were rather accurate with a maximum step length given as 0.05 of the total range; the CPU time per electron was 0.0045 s and the errors 1–2% for 200 000 source particles. For the thicker foils results are not so good, even if still reasonably satisfactory. Smaller values of the step length should appreciably reduce the discrepancy. The CPU time was 0.012 s per electron and the errors less than 2% for 150 000 source particles. The angular distribution of electrons transmitted by and reflected from the Cu foil given in fig. 8 was calculated with a maximum step length given as 0.05 of the total range; 250 000 particles were run to obtain errors less than 2% and the CPU time was 0.015 s per electron.

6.2.4. Benchmark 7

The calculated energy spectra (see fig. 8) for the three Al foils of the previous benchmark were less sensitive to the step size and are reasonably in agreement with the experimental data, taking account the fact that MCNPE-BO does not contain Landau fluctuations. The better agreement of FLUKA at the tail is due to the fact that with MCNPE-BO a higher value for the electron production threshold energy (50 keV) was used. The errors are of the order of a few percent for the same CPU time and the same parameters as were used for the angular distributions in benchmark 5.

6.2.5. Benchmark 8

The number reflection coefficient for electrons incident perpendicularly on an aluminium foil of saturation thickness (fig. 9) was calculated with a maximum step length given as 0.05 of the total range, though for energies greater than 1 MeV larger steps could be used. The time per electron depends on the energy of the electrons and ranges from 0.055 s for $E = 30$ keV to 0.45 s for $E = 20$ MeV; the errors were 1–2% for energies below 2.5 MeV, and a few percent for the higher energies.

7. Conclusions

The tests carried out with FLUKA show that the new transport algorithm is a powerful tool for extending the capabilities of the code and represents a substantial improvement over the standard EGS4 one previously adopted for e^+, e^-. The weak dependence of the results on the input parameters makes the code easy to use for an unspecialized user, and this was one of the major goal of this work.

Also the comparison of MCNPE-BO with experimental data is satisfactory so far and the solutions adopted in the code look promising. The code is still under development and more benchmarks are necessary before arriving at a definitive version.

Although more extensive tests are needed for an ultimate assessment on the validity of the model outlined in section 3, the presented comparison are very encouraging.

Acknowledgement

The authors wish to thank Dr. K.W. Burn for the many fruitful discussions and for help in revising this manuscript.

References

[1] P. Aarnio, A. Fassò, A. Ferrari, H.J. Moehring, J. Ranft, P.R. Sala, G.R. Stevenson and J.M. Zazula, FLUKA92 User Manual, to be published;
see also A. Ferrari, P.R. Sala, A. Fassò and G.R. Stevenson, Can we predict radiation levels in Calorimeters?, Invited paper presented at the II International Conference on Calorimetry in High Energy Physics, Capri, October 14–18 1991, proceedings in press.
[2] W.R. Nelson, H. Hirayama and D.W.O. Rogers, report SLAC-265 (1985).
[3] G.Z. Molière, Z. Naturforsch. 3a (1948) 78.
[4] G.Z. Molière, Z. Naturforsch. 10a (1955) 177.
[5] H.A. Bethe, Phys. Rev. 89 (1953) 1256.
[6] S. Goudsmit and J.L. Saunderson, Phys. Rev. 57 (1940) 24;
S. Goudsmit and J.L. Saunderson, Phys. Rev. 58 (1940) 36.
[7] L. Eyges, Phys. Rev. 74 (1948) 1534;
C.M. Yang, Phys. Rev. 84 (1951) 599;
see also B. Rossi and K. Greisen, Rev. Mode. Phys. 13 (1941) 267.
[8] A.F. Bielajew and D.W.O. Rogers, National Research Council of Canada report PIRS-0042 (1986); and Nucl. Instr. and Meth. B18 (1987) 231.
[9] D.W.O. Rogers, Nucl. Instr. and Meth. 227 (1984) 535.
[10] G. Lindstroem et al., report DESY 89-104 (1990).
[11] P.K. Job, G. Sterzenbach and D. Filges, Nucl. Instr. and Meth. A271 (1988) 442.
[12] A.F. Bielajew and D.W.O. Rogers, in: Monte Carlo Transport of Electrons and Photons, eds. T.M. Jenkins, W.R. Nelson and A. Rindi (Plenum, 1988) pp. 115–137; see also pp. 323–341.
[13] W.T. Scott, Rev. Mod. Phys. 35 (1963) 231.
[14] S.M. Seltzer, in: Monte Carlo Transport of Electrons and Photons, eds. T.M. Jenkins, W.R. Nelson and A. Rindi (Plenum, 1988) pp. 158–160.

[15] M.J. Berger, Methods in Computational Physics, vol. 1 (Academic Press, New York, 1963) p. 135.
[16] PDG, Review of Particle Properties, Phys. Lett. 239B (1990) p. III.14, and references therein.
[17] M.J. Berger and R. Wang, in: Monte Carlo Transport of Electrons and Photons, eds. T.M. Jenkins, W.R. Nelson and A. Rindi (Plenum, 1988) p. 21–56;
see also M.J. Berger, Appl. Radiat. Isot. 42 (1991) 905.
[18] P.A. Aarnio, J. Lindgren, J. Ranft, A. Fassò and G.R. Stevenson, CERN Divisional report TIS-RP/168 (1986);
see also J. Ranft, H.J. Moehring, T.M. Jenkins and W.R. Nelson, report SLAC-TN-86-3 (1986).
[19] R. Guaraldi and F. Padoani, MCNPE-BO User Manual, to be published.
[20] Group X-6, MCNP-A General Monte Carlo Code for neutron and photon transport. Version 3A, Los Alamos National Lab. report LA-7396-M rev. 2 (1981).
[21] M.J. Berger, in: Monte Carlo Transport of Electrons and Photons, eds. T.M. Jenkins, W.R. Nelson and A. Rindi (Plenum Press, 1988) p. 207, and references therein.
[22] K.R. Shortt, C.K. Ross, A.F. Bielajew and D.W.O. Rogers, Phys. Med. Biol. 1 (1986) 235.
[23] D.H. Rester and J.H. Derrickson, J. Appl. Phys. 42 (1971) 714.
[24] H. Frank, Z. Naturforsch. 14a (1959) 247.
[25] S.M. Seltzer and M.J. Berger, Nucl. Instr. and Meth. 119 (1974) 157;
see also M.J. Berger, in: Monte Carlo Transport of Electrons and Photons, eds. T.M. Jenkins, W.R. Nelson and A. Rindi (Plenum, 1988) p. 198.
[26] P. Verdier and F. Arnal, Compt. Rend. ser B267 (1968) 1443.
[27] G. Neubert and S. Rogaschewski, Phys. Status Solidi A59 (1980) 35.
[28] H. Dresher, L. Reimer and H. Seidel, Z. Angew. Phys. 29 (1970) 331.
[29] H.E. Bishop, in: Optique des Rayons X et Microanalyse, eds. R. Castaing, P. Deschamps and J. Philibert (Hermann, Paris, 1966) p. 153.
[30] D.H. Rester and J.H. Derrickson, Nucl. Instr. and Meth. 86 (1970) 261.
[31] A.J. Cohen and K.F. Koral, NASA Technical Note TN D-2782 (1965) cited after ref. [25].
[32] W.E. Miller, NASA Technical Note TN D-5724 (1970) cited after ref. [25].
[33] K.A. Wright and J.G. Trump, J. Appl. Phys. 33 (1962) 687.
[34] T. Tabata, Phys. Rev. 162 (1967) 337.

Edito a cura dell'ENEA, Direzione Relazioni Esterne
Viale Regina Margherita, 125 - Roma
Finito di stampare nel mese di dicembre 1993
presso il Laboratorio Tecnografico